cGAS-STING Signaling Pathway Mediates Brain Trauma-Induced Type I Interferon Response

Lauren Fritsch
Virginia Tech: Virginia Polytechnic Institute and State University
Jing Ju
Virginia Tech: Virginia Polytechnic Institute and State University
Erwin Kristobal Gudenschwager Basso
Virginia Tech: Virginia Polytechnic Institute and State University
Eman Soliman
Virginia Tech: Virginia Polytechnic Institute and State University
Swagatika Paul
Virginia Tech: Virginia Polytechnic Institute and State University
Jiang Chen
Virginia Tech: Virginia Polytechnic Institute and State University
Elizabeth Kowalski
Virginia Tech: Virginia Polytechnic Institute and State University
Taylor C Tuhy
Virginia Tech: Virginia Polytechnic Institute and State University
Rachana D Somaiya
Virginia Tech: Virginia Polytechnic Institute and State University
Xia Wang
Virginia Tech: Virginia Polytechnic Institute and State University
Irving C Allen
Virginia Tech: Virginia Polytechnic Institute and State University
Michelle H Theus (mtheus@vt.edu)
Virginia Tech: Virginia Polytechnic Institute and State University https://orcid.org/0000-0001-6485-2104
Alicia M Pickrell
Virginia Tech: Virginia Polytechnic Institute and State University

Research Article

Keywords: cGAS-STING, CCI, TBI, Inflammation

Posted Date: September 2nd, 2021

DOI: https://doi.org/10.21203/rs.3.rs-855949/v1

cGAS-STING signaling pathway mediates brain trauma-induced Type I Interferon response

Lauren E. Fritsch[1], Jing Ju[2], Erwin Kristobal Gudenschwager Basso[3], Eman Soliman[3], Swagatika Paul[4], Jiang Chen[2,6], Elizabeth J.A. Kowalski[3] , Taylor C. Tuhy[5], Rachana Deven Somaiya[1], Xia Wang[3], Irving Coy Allen[3], Michelle H. Theus[3,5 #], and Alicia M. Pickrell[5, #]

[1]Translational Biology, Medicine, and Health Graduate Program, Virginia Polytechnic Institute and State University, Roanoke, VA 24016 USA
[2]Molecular and Cellular Biology Graduate Program, Virginia Polytechnic Institute and State University, Blacksburg, VA 24061, USA
[3]Department of Biomedical Sciences and Pathobiology, Virginia Polytechnic Institute and State University, Blacksburg, VA 24061, USA
[4]Biomedical and Veterinary Sciences Graduate Program, Virginia Polytechnic Institute and State University, Blacksburg, VA 24061, USA
[5]School of Neuroscience, Virginia Polytechnic Institute and State University, Blacksburg VA 24061, USA
[6]Present address: Sorrento Therapeutics, Inc., 4955 Directors Place, San Diego, CA 92121

Correspondence should be addressed to:

Alicia M. Pickrell, 970 Washington Street SW, Life Science I Rm 217, Blacksburg, VA 24061
Tel: 540-232-8465; Fax: 540-231-1475; Email: alicia.pickrell@vt.edu
Michelle H. Theus, 970 Washington Street SW, Life Science I Rm 245, Blacksburg, VA 24061
Tel. 540-231-0909; Fax 540-231-7425; Email: mtheus@vt.edu**Keywords**

brain injury, inflammation, interferons, STING, cGAS, innate immunity

Abstract

Background: Inflammation is a key contributor of neuronal death and dysfunction following traumatic brain injury (TBI). Recent evidence suggests that interferons may be a key regulator of this response. Our studies evaluated the role of the Cyclic GMP-AMP Synthase-Stimulator of Interferon Genes (cGAS-STING) signaling pathway a murine model of TBI.

Methods: Male, eight-week old wildtype, *STING* knockout ($^{-/-}$), *cGAS*$^{-/-}$, and *NLRX1*$^{-/-}$ mice were subjected to controlled cortical impact (CCI) or sham injury. Histopathological evaluation of tissue damage was assessed using non-biased stereology, which was complemented by analysis at the mRNA and protein level using qPCR and western blot analysis, respectively.

Results: We found that STING and Type I interferon-stimulated genes were upregulated after CCI injury in a bi-phasic manner and that loss of cGAS or STING conferred neuroprotection concomitant with a blunted inflammatory response at 24 hours post-injury. cGAS$^{-/-}$ animals showed reduced motor deficit 4 days after injury (dpi), and amelioration of tissue damage was seen in both groups of mice up to 14 dpi. Given that cGAS requires a cytosolic damage- or pathogen- associated molecular pattern (DAMP/PAMP) to prompt downstream STING signaling, we further show that mitochondrial DNA is present in the cytosol after TBI. Finally, our findings demonstrate that NLRX1 may be an additional regulator that functions upstream to regulate cGAS-STING pathway.

Conclusions: These findings suggest that the canonical cGAS-STING-mediated Type I interferon signaling axis is a critical component of neural tissue damage following TBI and that mtDNA may be a possible trigger in this response.

Introduction

Traumatic brain injury (TBI) is a complex neurological condition that is a leading cause of death and disability in children and adults [1]. Injury occurs in two phases: an initial, acute mechanical injury resulting from the external force, and secondary injury/cell death due to complications such as hypoxia, ischemia, and inflammation [2,3]. While the use of improved safety measures has helped minimize the severity of the initial impact, little progress has been made in understanding or treating secondary injuries.

Neuroinflammation is a key mediator of secondary brain injury; however, anti-inflammatory pharmacological approaches largely fail in clinical trials [4]. Interferons (IFNs) are elevated in post-mortem humans TBI samples (IFN-γ) [5,6] and in experimental TBI murine models (IFN-α, IFN–β, IFN–γ) [6,7], but their functional role has been understudied in TBI. Interferons are produced in response to detection of pathogen associated molecular patterns (PAMPs) by pattern recognition receptors (PRRs) [8]. Upon detection of pathogenic nucleic acids, PRRs trigger the production of Type I IFNs to prime both the affected and adjacent cells for pathogen attack. While a number of subtypes of Type I IFNs have been identified, IFN-α and IFN-β are most well-studied [9]. These IFNs act via binding to the cell surface complex known as IFN-α/β receptor (IFNAR), resulting in expression of IFN-stimulated genes (ISGs) via the JAK-STAT pathway [10].

The endoplasmic reticulum protein, STimulator of INterferon Genes (STING), is known to trigger Type I IFN responses after being activated by cyclic guanosine monophosphate-adenosine monophosphate (cGAMP), a second messenger produced by the DNA sensor cyclic GMP-AMP synthase (cGAS) [11,12]. cGAS is able to bind nuclear and mitochondrial DNA

[13,14] to promote STING activation and subsequent translocation of transcription factors [15,16], resulting in the production of innate immune genes, including IFNs and ISGs [17].

Previous studies have demonstrated that STING mRNA is elevated in post-mortem human TBI brain samples, and genetic loss of STING or IFNAR in murine models of TBI reduces lesion size and autophagy markers [6,18]. Pharmaceutical inhibition of cGAS, the upstream mediator of STING, in a murine stroke model reduced microglial activation and peripheral immune cell infiltration [19]. Interferon signaling is gaining increasing attention for it role in mediating progressive damage in TBI [20,21]. Taken together, this suggests that cGAS-STING signaling may represent a novel mechanism controlling post-traumatic neuroinflammation; however, there is evidence of non-canonical, cGAS-independent STING activation, particularly in response to DNA damage [22,23]. Because upstream STING signaling is undefined in the brain, clarifying the mechanisms of STING activation in the context of sterile inflammation is critical for identifying targets for therapeutic intervention.

In this study, we utilized genetic knockout mouse models to elucidate the role of the cGAS-STING signaling pathway after TBI in a preclinical model of controlled cortical impact (CCI) injury. We report that the ISG response is immediately upregulated after injury and provide evidence that the presence of cytoplasmic mtDNA is available for cGAS binding in the injured cortex. In addition to confirming that loss of endogenous STING is protective [18], our data suggests that canonical cGAS-STING signaling is a critical component of trauma-induced neuroinflammation and tissue damage. We also uncover *in vivo* evidence first the first time, that nucleotide-binding oligomerization domain, leucine rich repeat containing X1 (NLRX1) abrogates this pathway in the brain. Taken together, we conclude canonical cGAS-STING signaling plays a necessary and sufficient role in TBI outcome.

Results

CCI injury induces a biphasic ISG response in the damaged cortex

Neuroinflammation is a critical component of the secondary injury response in TBI and offers a number of potential therapeutic targets, but is highly complex and remains poorly understood [24]. To provide further insight into how TBI alters inflammatory gene transcription in a temporal manner, we first sought to broadly profile changes in cytokines, PRRs, ISGs, IFNs, and transcription factors known to be upregulated by the innate immune system [25]. Cortices from male 8-week injured mice showed that a temporally biphasic increase in mRNA expression for most (10 of 13) genes tested compared to shams (Figure 1a-c). Expression of *Il-10, MCP-1, RIG-I, CXCL10, IFIT1, IFIT3, IFNA4, IFNB1, IRF7,* and *STAT1* was significantly increased at 2- and 24-hours (hrs) post injury, which was blunted at 4hrs. *IFIH1* (also known as MDA5), and *STAT2* expression was unchanged. Furthermore, *Il10, MCP1* and *Il-6* did not show a biphasic expression pattern. Of note, the Type I IFNs IFNA4 and IFNB1 showed biphasic upregulation after injury.

Previous reports demonstrate neuroprotection in *STING*$^{-/-}$ mice after CCI injury [18]. To gain a more in-depth understanding of the expression pattern of STING, we assessed mRNA levels at 2, 4, and 24hrs in the ipsilateral parietal cortex (Figure 1d). We find *STING* is upregulated at all time points tested but shows the greatest change in expression at 2 and 4hrs post-injury (Figure 1d). Interestingly, STING itself is an ISG and is positively regulated by its own transcription upon activation [26]. Taken together, these data demonstrate a strong innate immune response occurring within hours after TBI.

CCI injury induces the presence of cytosolic mitochondrial DNA in damaged cortex

Loss of STING [18], IFNAR [6], or IFNβ [20,21] function has been shown to be beneficial in TBI outcome; however, the mechanism regulating their induction remains unclear. The canonical STING-cGAS pathway is activated by binding of viral nucleic acids found in the cytoplasm [14], resulting in production of the second messenger cGAMP which binds and activates STING [11,12]. In addition, mitochondrial DNA (mtDNA) can activate STING in models where mtDNA packaging proteins and mitochondrial permeability proteins are disrupted genetically [13,27] and it is present in cerebral spinal fluid and serum following TBI [28,29].

To determine whether mtDNA is present in the cytoplasm, we isolated the cytoplasmic fraction of cells isolated from the ipsilateral cortex. We used primers that targeted two different locations on the mitochondrial genome corresponding to the coding region for COX1 and ND1 (Figure 2a). To ensure that our cytosolic fractions were enriched, western blotting detected the presence of the cytosolic protein α-tubulin but was devoid of the nuclear and outer mitochondrial membrane protein histone H3 and Mfn2 (Figure 2b). Interestingly, we saw a significant elevation in mtDNA at 2hrs (Figure 2c), and 4hrs (Figure 2d) post-injury, which was resolved by 24hrs (Figure 2e), indicating that mtDNA is present in the cytoplasm of the injured cells. These data correlated with ISG induction at 2hrs post-injury (Figure 1a).

To determine whether cytoplasmic nuclear DNA was also present, we performed western blotting on cytoplasmic extracts at the 2hrs to evaluate the expression of the nuclear protein high mobility group box protein 1 (HMGB1), whose expression is increased when nuclear DNA is present in the cytosol [30,31]. cGAS also is more easily bound to and activated by HMGB1 coated nuclear DNA than in its free form [32]. We found HMGB1 was present in cytosolic fractions isolated from both contralateral and ipsilateral hemispheres (Figure 2f); however, ipsilateral cytoplasmic HMGB1 expression was not increased compared to contralateral (Figure 2g). This

suggests that mtDNA is more likely to drive cGAS activation in the damaged cortex after CCI injury.

Loss of cGAS-STING confers neuroprotection after CCI injury

cGAS is necessary for canonical STING activation [14,34]. To verify this pathway involvement in TBI, we utilized cGAS KO mice (*cGAS*$^{-/-}$; Supplemental Figure 1a) and STING KO (*STING*$^{-/-}$; Supplemental Figure 1b) mice. *STING*$^{-/-}$ mice displayed a significant reduction in lesion volume compared to WT at 1 day post-injury (dpi) (Figure 3a, 3c), confirming prior work [18]. Moreover, *cGAS*$^{-/-}$ mice also showed significant neuroprotection (Figure 3a, 3d) compared to WT mice (Figure 3a, 3b). To determine whether a reduction in lesion volume was due to increased neuronal survival, we performed immunodetection of apoptotic neurons by TUNEL staining (Figure 3h). TUNEL detects nuclear DNA fragmentation, a hallmark of apoptosis and necrosis [37]. A significant reduction of TUNEL^{+} cells was detected 24hrs after injury in both *cGAS*$^{-/-}$ and *STING*$^{-/-}$ mice (Figure 3e). Co-labeling with Nissl, an unspecific neuronal marker, showed the number of apoptotic neurons was significantly reduced in the ipsilateral cortex of *STING*$^{-/-}$ mice after injury and trending toward a significant reduction in cGAS$^{-/-}$ mice (Figure 3f). Although cGAS/STING deficiency is neuroprotective, no difference was observed on blood-brain barrier function as seen by quantifying Evans Blue infiltration in the damaged cortex compared to contralateral (Figure 3g). Our results suggest that the cGAS-STING pathway contributes to the neurotoxic effects induced by CCI injury.

Behavioral impairments have been previously assessed in *IFNβ*$^{-/-}$ mice after TBI [20], therefore we sought to provide further confirmation that canonical cGAS-STING signaling is critical in TBI outcome. Using rotarod assessment, we found no difference in motor function

between sham-injured *cGAS*$^{-/-}$ and WT mice (Supplemental Figure 2a). However, *cGAS*$^{-/-}$ mice showed a significant reduction in motor deficit at 4dpi compared to WT (Supplemental Figure 2b) but no difference at 7 and 14dpi (Supplemental Figure 2b). *cGAS*$^{-/-}$ mice also showed a significant reduction in lesion volume at 14dpi relative to WT (Supplemental Figure 2c-d), despite their comparable motor performance (Supplemental Figure 2b). Similarly, *STING*$^{-/-}$ mice also showed reduced lesion volume at 14dpi (Supplemental Figure 2c-d). We also assessed mRNA levels of IFNA4, IFNB1, and IL-6 at 14 days post-injury. Interestingly, all three genes were downregulated at this chronic timepoint relative to WT sham animals (Supplemental Figure 4e).

Loss of cGAS-STING ameliorates pro-inflammatory gene expression after CCI injury

In addition to histological and functional changes, we profiled changes in gene expression in the cortex at 24hrs post-injury in WT, *STING*$^{-/-}$, and *cGAS*$^{-/-}$ mice. We found no difference in the contralateral cortex when compared to sham (Supplemental Figure 3), therefore we used contralateral tissue when performing our relative analysis. Both *STING*$^{-/-}$, and *cGAS*$^{-/-}$ mice showed a significant reduction in mRNA expression of *Il10, Il6, MCP1, IFNA4,* and *IFNB1* (Figure 4a-e) in the ipsilateral cortex when compared to WT. To provide further insight into the transcriptional changes, we assessed the complete panel of genes described in Figure 1. We found all genes tested were significantly altered in *STING*$^{-/-}$ mice compared to WT (Supplemental Figure 4). These finding sugget cGAS-STING signaling plays a key role in regulating innate immune gene expression in the damaged cortex after CCI injury.

Microglia are the predominant cell type expressing cGAS and STING in the brain

There is conflicting evidence regarding which CNS cell types express cGAS and STING [18,19,41,42]. To test this, we employed several techniques for isolating pure CNS cell populations

for qPCR assessment. Naïve astrocytes and endothelial cells were extracted using magnetic bead sorting [43,44], while the remaining cells were plated for isolating microglia and primary neuronal cultures were used to assess expression in neurons. Real-time qPCR analysis of cell-type specific genes was used to verify purity of the isolated cell populations (Figure 5a). We observed that microglia showed the greatest enrichment of transcripts for both *cGAS* and *STING*, when compared to all other cell types, (Figure 5b-c). This suggests that microglia may represent the main cell source influencing the type I interferon response via cGAS-STING pathway in TBI.

NLRX1 negatively regulates cGAS-STING activation after CCI injury

We recently show that loss of NLRX1 exacerbates tissue damage after CCI injury, in part, by increasing NF-κB activity in microglial and/or peripheral-derived immune cell [45]. It is also well-established that NLRX1 may sequester STING to prevent the interferon response [46], however, this association has not been evaluated in the brain. To test whether NLRX1 represents a novel upstream regulator of STING in the cortex after injury, we evaluated activated STING expression and the ISG response. Interestingly, *NLRX1*$^{-/-}$ mice showed a significant increase in activated (phosphorylated) p-STING (S365) compared to WT at 3dpi (Figure 5a-b). We also assessed mRNA expression of *IL-10, IL-6, MCP1, IFNA4,* and *IFNB1* 24hrs post-injury. Relative to WT, *NLRX1*$^{-/-}$ mice showed a significant increase in cortical expression of all genes tested, importantly ISG *IFNA4* and *IFNB1* (Figure 5c-g). These data suggest that NLRX1 plays a central role in suppressing the type I interferon response by limiting STING activation following CCI injury.

Discussion

Our data suggests that the antiviral interferon pathway mediated by cGAS-STING contributes to the secondary injury after TBI. The activation of STING in the nervous system has recently been brought to the attention of those studying CNS viral infections. STING is highly conserved among organisms [47,48] and restricts Zika infection in the *Drosophila* brain [49]. Microglial expression and activation of STING also restricts herpes simplex virus-1 (HSV-1) infection in neurons or promote apoptosis, depending on viral load [50,51]. However, the classical viral/microbe induced innate immune pathways in the brain may not necessarily need viral induced stimulation for activation. In mouse models of multiple sclerosis, a demyelinating neurodegenerative disease, STING may control microglial reactivity [52].

The present work demonstrates that STING is upregulated in the ipsilateral cortex of CCI-injured mice, which correlates with a biphasic increase in a variety of cytokines, including IFNA4 and IFNB1. While previous work has shown that loss of endogenous STING reduces lesion size following TBI [18], recent evidence suggests that STING may be able to function independently of its canonical upstream mediator, cGAS [22,35,36,53]. Therefore, this study sought to determine the effects of cGAS deficiency and to identify a potential DAMP that may influence the induction of the canonical cGAS-STING pathway in CCI injury. Our data shows that cGAS and STING are highly expressed in microglia and that *cGAS*$^{-/-}$ mice display significant neuroprotection and a blunted ISG response, similar to *STING*$^{-/-}$ mice. This correlates with the observation of cytoplasmic mtDNA in the damaged cortex and suggests mtDNA is a possible DAMP that induces cGAS-STING pathway in microglia leading to type I interferon-induced tissue damage in TBI. Moreover, we demonstrate that NLRX1 is a novel upstream regulator of STING in this response.

Our study selected a panel of genes associated with the Type I interferon response, including pro-inflammatory (IL-6), anti-inflammatory (IL-10), and pro-immune migratory (MCP-1) cytokines, as well as transcription factors (STAT1, STAT2, and IRF7), interferons (IFNA4 and IFNB1), and ISGs (CXCL10, IFIT1, IFIT3, and IFIH1). We determined that loss of cGAS or STING resulted in a broadly blunted immune response 24hrs after injury. Recent work has suggested that STING simultaneously stimulates the production of pro- and anti-inflammatory cytokines to facilitate maintenance of gut homeostasis [55], and studies in mouse models of systemic lupus erythematosus (SLE) have indicated STING signaling can be pro- or anti-inflammatory depending on the model [56–58]. Still, the autoimmune syndrome SAVI that results from gain-of-function mutations in STING results in excessive inflammation, indicating a primarily pro-inflammatory role for STING [59]. Our data shows altered mRNA expression of both pro- and anti-inflammatory cytokines in *cGAS*$^{-/-}$ and *STING*$^{-/-}$ mice, suggesting that the effects of cGAS-STING signaling is highly complex and likely context-dependent. Further, the unselective upregulation of mRNAs for proteins with predominantly antiviral roles, such as IFIT1 and IFIT3, suggests that this innate immune pathway is activated aberrantly after injury, unlike its normal role in viral or bacterial clearance. Further investigation is needed to clarify how the balance of pro- and anti-inflammatory cytokines is disrupted or skewed by alterations in cGAS-STING activity.

Recent findings show that mRNA expression of STING and key ISGs are elevated up to 60 days after experimental TBI [20], indicating that STING activity may also contribute to chronic neuroinflammation. Consistently, we found that *cGAS*$^{-/-}$ mice showed reduced motor deficits compared at 4dpi and reduced lesion volume up to 14 days post-injury. Interestingly, we found that the type I interferon ISG response was significantly reduced by 4dpi (data not shown), and

entirely resolved at 14 days. These data suggest that while the cGAS-STING signaling axis is acutely activated after injury, additional subsequent mechanisms may further contribute to the chronic progression on injury after trauma [60]. Further work is needed to define the temporal dynamics of cGAS-STING signaling after TBI.

Conflicting evidence exists regarding whether NF-κB signaling is a major pathway activated downstream of STING [61–64]. However, recent work in mice with a point mutation in STING (S365A) that interfered with IRF3 binding elucidated that the switch between NF-κB signaling and Type I interferon signaling was context-dependent [65]. With the generation of these STING point mutation mouse models, future work could further define the contribution of different downstream effects of STING during TBI. Yet, Type-1 IFN receptor (IFNAR1) knockout mice are protected from TBI injury [6] indicating that the interferon pathway is still a major contributor to neuroinflammation in TBI. However, future work is needed to elucidate cell-type specific effects mediating the IFN response to TBI.

While our findings demonstrate the presence of cytosolic mtDNA, it is remains unclear how it is released into the cytosol after injury. Recently, the DNA/RNA binding protein TDP-43 has been implicated in the release of mtDNA via the mitochondrial permeability transition pore (mPTP) and subsequent cGAS-STING activation in a mouse model of ALS [66]. Other work has shown that BAK/BAX macropores facilitate mitochondrial herniation and mtDNA efflux independent of the mPTP [27,67]. Mechanical forces have been shown to promote mitochondrial fission events [68] that may allow for mtDNA release; indeed, TBI is associated with increases in mitochondrial fission and the fission-initiating dynamin-related protein 1 (Drp1) [69]. Clarifying how mtDNA is released following neurotrauma may offer alternative therapeutic targets for reducing cGAS-STING-mediated neuroinflammation.

Taken together, these data confirm that STING-mediated IFN signaling is detrimental to TBI-induced tissue damage. We have shown that loss of cGAS or STING results in improved histological and functional measures up to 14 days after TBI. Additionally, we provide evidence that NLRX1 negatively regulates STING activation in the brain, offering an additional potential target for therapeutic intervention. Perhaps most significantly, this study is the first to investigate mtDNA as a possible trigger for STING-IFN signaling in neurotrauma. Overall, our findings indicate that the canonical cGAS-STING-mediated ISG response is an early neuroinflammatory event occurring after cortical trauma, which represents a novel therapeutic target for treatment.

Material and Methods

Animals

All mice were housed in pathogen-free facility on a 12-hour light/dark cycle at Virginia Tech and provided standard rodent diet and water *ad libitum*. Male CD-1, C57BL/6J (wildtype), C57/Bl/6J-TMEM173^{gt}/J (STING$^{-/-}$) [73], and B6(C)-*Cgas*$^{tm1d(EUCOMM)Hmgu}$/J (cGAS$^{-/-}$) mice were purchased from Jackson Laboratories (Ellsworth, ME, USA). NLRX1$^{-/-}$ mice were previously described [74]. *STING*$^{-/-}$, *cGAS*$^{-/-}$, and *NLRX1*$^{-/-}$ mice were genotyped according to protocols provided by Jackson Laboratories. All experiments were conducted in accordance with the NIH Guide for the Care and Use of Laboratory Animals and under approval of the Virginia Tech Institutional Animal Care and Use Committee.

Controlled cortical impact (CCI) injury

Animals were prepared for surgery as previously described [75]. Male CD-1, wildtype, STING$^{-/-}$, cGAS$^{-/-}$, and NLRX1$^{-/-}$ mice age 8-10 weeks were anesthetized with an intraperitoneal injection of ketamine (100 mg/kg) and xylazine (10 mg/kg), then positioned in a stereotactic frame.

Body temperature was continually monitored via rectal probe and maintained at 37°C with an autoregulated heating pad. A 4 mm craniotomy was made with a portable drill over the right parietal-temporal cortex (-2.5 mm A/P and 2.0 mm lateral from bregma). Moderate CCI was induced with an eCCI-6.3 device (Custom Design and Fabrication, Richmond, VA, USA) using a 3 mm impact tip at an angle of 70°, 5.0 m/s velocity, 2.0 mm impact depth, and 100 ms dwell period [76]. The incision was closed with Vetbond tissue adhesive (3M, St. Paul, MN, USA), and post-surgery animals received Buprenorphine SR (1 mg/kg, ZooPharm, Windsor, CO, USA) subcutaneously. Sham animals received a craniotomy only.

Histology and TUNEL staining

At the indicated times post-CCI injury, mice were anesthetized by isoflurane (IsoFlo®, Zoetis, Parsippany-Troy Hills, NJ, USA) and euthanized by cervical dislocation. Brains were fresh frozen on dry ice while embedded in O.C.T. (Tissue-Plus™ O.C.T. Compound, Fisher HealthCare, Houston, TX, USA). Brains were coronally sectioned (30 µm thickness) using a cryostat (CryoStar NX50, Thermo Scientific, Waltham, MA, USA) through the lesion site (-1.1 to -2.6 mm posterior to bregma). Serial sections 300 µm apart were stained with Cresyl violet (Electron Microscopy Sciences, Hatfield, PA, USA).

To identify cells undergoing apoptosis, slides were fixed in 10% formalin (Fisher Chemicals, Pittsburgh, PA) for 5 min, washed with 1X PBS, permeabilized in 2:1 ethanol:acetic acid at -20°C for 10 minutes and 0.4% Triton for 5 minutes, then washed with 1X PBS and TUNEL stained according to the manufacturer's suggestions (DeadEnd™ Fluorometric TUNEL System, Promega, Madison, WI). Slides were then fixed for 5 minutes in 10% formalin, blocked for 30 minutes in 0.2% Triton, 2% cold water fish gelatin (Sigma, St. Louis, MO, USA), and stained for Nissl (1:100, NeuroTrace™ 530/615 Red Fluorescence Nissl, Invitrogen, Carlsbad, CA, USA).

Slides were mounted with DAPI Fluoromount-G (SouthernBiotech, Birmingham, AL, USA). Representative confocal images were taken on a Nikon C2 at 20x magnification using the recommended z-step size. Maximum intensity projections were created in Nikon NIS-Elements.

Estimating lesion size and TUNEL$^+$/Nissl$^+$ cells

Lesion volume (mm^3) was assessed by a blinded investigator using StereoInvestigator's Cavalieri estimator (MicroBrightField, Williston, VT, USA) and an Olympus BX51TRF motorized microscope (Olympus America, Center Valley, PA, USA), as previously described [45]. Five coronal serial sections for each animal were spaced 300 µm apart surrounding the epicenter of injury were stained for Nissl (described above) and viewed at 4x magnification under brightfield illumination. A grid (100 µm spacing) was set over the ipsilateral lesion site and markers were placed over the contused tissue, as identified by diminished Nissl staining intensity, morphology, and pyknotic neurons. The contoured area with the section thickness, section interval, and number of sections were used by the Cavalieri program to estimate volume of contused tissue.

Apoptotic cells (TUNEL$^+$) were counted by a blinded investigator using five adjacent coronal serial sections (spaced 300 µm apart) with the StereoInvestigator Optical Fractionator (MicroBrightField, Williston, VT, USA) probe. Approximately 100 randomized sites per animal (grid size: 500 x 500 µm, counting frame size: 100 x 100 µm) were assessed to identify TUNEL$^+$ and TUNEL$^+$/Nissl$^+$ cells (apoptotic neurons), and section thickness was estimated every 5 sites to improve accuracy of the cell count estimation. The number of cells per contour, average estimated section thickness, section interval, and number of sections were used to estimate the number of cells within the lesion volume.

Real Time qPCR

A 4x4mm section of the injured cortex tissue was micro-dissected from each animal and immediately submerged in TRIzol™ Reagent (Invitrogen, Carlsbad, CA, USA). Either sham surgery animals' parietal cortices or the contralateral parietal cortex from injured animals were extracted to serve as the control. Cortical tissue was mechanically homogenized, lysed, and extracted with TRIzol™ Reagent (Invitrogen, Carlsbad, CA, USA) following the manufacturer's protocol. RNA was reverse transcribed to cDNA using iScript cDNA Synthesis Kit (Bio-Rad, Hercules, CA, USA). Reactions containing SYBR Green PCR Master Mix (Bio-Rad, Hercules, CA, USA), 10-50 ng of cDNA and 0.4 mM of each primer set was run on the CFX96 System (Bio-Rad, Hercules, CA, USA). qPCRs were performed in technical triplicates for each gene/primer set (Table 1). Expression levels were normalized to GAPDH and fold change was determined by comparative C_T method [77]. Primer efficiency was determined using a 4-point log concentration curve (Bio-Rad CFX Maestro software, Hercules, CA, USA).

Gene	Forward Seq. (5' - 3')	Reverse Seq. (5' - 3')
IRF7	CAA TTC AGG GGA TCC AGT TG	AGC ATT GCT GAG GCT CAC TT
IFIT1	ACC ATG GGA GAG AAT GCT GAT G	TGT GCA TCC CCA ATG GGT TC
STAT1	GCG GCA TGC AAC TGG CAT ATA ACT	ATG CTT CCG TTC CCA CGT AGA CTT
STAT2	TGA TCT CTA ACA GAC AGG TGG	CTG CAT TCA CTT CTA AAG ACT C
IFIT3	ATC ATG ATG GAG GTC AAC CG	TTG CAC ACC CTG TCT TCC AT
IFNA4	CTT TCC TCA TGA TCC TGG TAA TGA T	AAT CCA AAA TCC TTC CTG TCC TCC
IFNB1	AAC TCC ACC AGC AGA CAG TG	GGT ACC TTT GCA CCC TCC AG
RIG-I	GAG TAC CAC TTA AAG CCA GAG	AAT CCA TTT CTT CAG AGC ATC C
IFIH1	CGG AAG TTG GAG TCA AAG C	TTT GTT CAG TCT GAG TCA TGG
IL-10	AGA CCAAGGTGTCTACAAGGC	TCA TCA TGT ATG CTT CTA TGC AGT
IL-6	CTA GCT CAG GCT CGT CAG TTC	CTA GCT CAG GCT CGT CAG TTC
MCP1	CTA GCT CAG GCT CGT CAG TTC	CTA GCT CAG GCT CGT CAG TTC
CXCL10	ATA ACC CCT TGG GAA GAT GGT G	CTA GCT CAG GCT CGT CAG TTC
GAPDH	ATT GTG TCC GTC GTG GAT CTG A	AGA TGC CTG CTT CAC CAC CTT CTT
STING	GCC TTC AGA GCT TGA CTC CA	GTA CAG TCT TCG GCT CCC TG

Table 1: qPCR primers used in experiments.

List of forward and reverse sequences used for qPCR>

Western Blot

A 4x4mm section of injured cortex tissue was micro-dissected from each animal, snap frozen in liquid nitrogen, and stored at -80°C until use. Extracts were homogenized with a hand-held mortar/pestle (VWR, Radnor, PA, USA) on ice in RIPA buffer (Thermo Scientific Pierce Protein Biology, Waltham, MA, USA) containing proteinase and phosphatase inhibitors (Thermo Scientific Pierce Protein Biology, Waltham, MA, USA). Homogenates were spun at 4°C at 15,000 x *g* for 15 minutes and the supernatant was stored at -80°C until use. Protein quantification was determined using the DC protein assay kit with BSA standards (Bio-Rad, Hercules, CA, USA). 50 mg of protein was run on a 4-12 percent NuPage Bis-Tris Gel (Thermo Fisher Scientific, Waltham, MA, USA) and transferred onto a PVDF membrane (MilliporeSigma, Burlington, MA, USA). Primary antibodies were incubated overnight. Primary antibodies used were p-STING S365, STING, cGAS, histone H3 (Cell Signaling Technology, Danvers, MA, USA), α-tubulin (MilliporeSigma, Burlington, MA, USA), Mfn2 (was a kind gift from Richard Youle's laboratory), HMGB1 (R&D Systems, Minneapolis, MN, USA), occludin (Santa Cruz Biotechnology, Dallas, TX, USA), and Claudin-5 (Invitrogen, Carlsbad, CA, USA). Membranes were washed in 1x TBST, and secondary HRP conjugated antibodies (Jackson ImmunoResearch Laboratories, Inc., West Grove, PA, USA) were incubated at RT for 1 hr. Chemiluminescent detection (Thermo Scientific Pierce Protein Biology, Waltham, MA, USA) was used to detect signal with the Bio-Rad ChemiDoc system (Bio-Rad, Hercules, CA, USA). Relative optical density was determined with ImageLab software (Bio-Rad, Hercules, CA, USA).

Evans Blue

Twenty-four hours after CCI injury, animals received an intravenous injection of 300 µL Evans blue. After 3 hours, animals were sacrificed, and ipsilateral and contralateral hemispheres were collected. Distribution of Evans Blue was verified by opening the thoracic and abdominal

cavities. Tissue was incubated in 500 µL 10% formamide at 55°C for 24 hours, then centrifuged for 4 minutes at 210 x *g* to pellet the tissue. Absorbance for each hemisphere was measured in triplicate at 610 nm.

Rotarod

Gross motor function was evaluated by Rotarod (Columbus Instruments, Columbus, OH, USA) testing from 4 to 14 days post-TBI. Initial velocity was 5 rpm, with an acceleration of 0.1 rpm/s. Each animal underwent three trials per day with a 2-minute rest between each trial. The average time of the three trials was used for analysis. Eight-week-old animals were trained for 4 consecutive days with a baseline measurement taken on the fifth day. Animals underwent sham or CCI surgery, then rotarod performance was evaluated at 4-, 7-, and 14-days post-surgery. Each animal's performance was compared to its baseline measurement, and average performance for all animals was reported. After the final day of testing, animals were euthanized for histology, qPCR, or western blotting as described above.

Cytosolic Fraction

The cytosolic fraction was extracted as previously reported [13]. Cortical tissue was homogenized in PBS plus protease and phosphatase inhibitors (Thermo Scientific Pierce Protein Biology, Waltham, MA, USA). Dissociated tissues were incubated in the cytosolic extraction buffer containing 150 mM NaCl, 50 mM HEPES, pH 7.4, and 15–25 µg/ml digitonin (Gold Biotechnology, St Louis, MO, USA). The homogenates were incubated end over end for 10 minutes to allow selective plasma membrane permeabilization, then centrifuged at 980 *g* for 3 min three times to pellet intact cells. Pellets were retained for western blotting. The supernatant was centrifuged 17000 *g* for 10 min to pellet any remaining cellular debris. DNA was extracted the Zymo DNA extraction kit.

411 *Cell isolations*

412 Murine cells were isolated using the Worthington Dissociation Kit (Worthington Biochemical
413 Corporation, Lakewood, NJ, USA) and slight modifications to published protocols [43,78].
414 Briefly, WT animals were deeply anesthetized with a ketamine (500 mg/kg)/xylazine (10 mg/kg)
415 cocktail and hand perfused with cold PBS to remove blood. The brain was removed, cortices
416 dissected, and finely minced in warmed papain with DNase. Tissue was digested in papain at 37°C
417 for 15 minutes for astrocytes and endothelial cells or 45 minutes for microglia with gentle
418 inversions every five minutes. For astrocytes and endothelial cells, the solution was titruated,
419 centrifuged at 300g for 5 mins 4°C, and the pellet was resuspended in resuspension buffer per the
420 Worthington protocol to stop the digestion. The dissociated cells were spun down again, filtered
421 through a 70µm cell strained with 10 mL 0.5% BSA PBS, then resuspended in 200 µL 0.5% BSA
422 PBS and microbeads. Oligodendrocytes were removed with anti-myelin beads, then endothelial
423 cells and astrocytes were isolated with CD31 and ACSA-2 beads (all microbeads from Miltenyi
424 Biotec, Auburn, CA, USA), respectively, per published protocols [43,78]. *Microglia:* Microglia
425 were isolated by plating the cells collected following the Worthington Papain Dissociation System
426 protocol. Cells were incubated for one hour at 37°C and non-adherent cells were washed off,
427 leaving microglia adherent to the plate. *Primary Neurons:* Primary neurons were isolated from P0
428 mouse pups per the Worthington Papain Dissociation System protocol and cultured on poly-d-
429 lysine-coated plates in Neurobasal Medium with B27 supplement (Gibco, Waltham, MA, USA).
430 Primary neurons were collected 14 days after plating for RNA isolation.

431 *Statistical analysis*

432 Data were analyzed with GraphPad Prism 9 (GraphPad, San Diego, CA, USA). A student's
433 two-tailed t-test was used for comparison of two experimental groups. One-way or two-way

ANOVA with Tukey's multiple comparison test was used for comparison of more than two experimental groups as appropriate. Differences were considered statistically significant at $p < 0.05$. Data reported as mean ± SEM. n values are reported in the figure legends.

Abbreviations

BBB, blood brain barrier; CCI, controlled cortical impact; CDN, cyclic dinucleotide; cGAMP, cyclic guanosine monophosphate-adenosine monophosphate; cGAS, cyclic GMP-AMP synthase; CNS, central nervous system; CXCL10, C-X-C motif chemokine ligand 10; DAMP, damage-associated molecular pattern; Drp1, dynamin-related protein 1; GAPDH, glyceraldehyde 3-phosphate dehydrogenase; IFIH, interferon-induced helicase C domain-containing protein; IFIT, interferon-induced proteins with tetratricopeptide repeats; IFN, interferon; IFNAR, interferon alpha/beta receptor; IL, interleukin; IRF, interferon response factor; ISG, interferon-stimulated gene; JAK-STAT, Janus kinase-signal transducer and activator of transcription; KO, knock out; MCP-1, monocyte chemoattractant protein 1; MMP, matrix metalloproteinase; mPTP, mitochondrial permeability transition pore; mtDNA, mitochondrial DNA; NF-kB, nuclear factor kappa-light-chain-enhancer of activated B cells; NLRX1, NOD-like receptor containing X1; PAMP, pathogen-associated molecular pattern; PRR, pattern recognition receptor; qPCR, quantitative polymerase chain reaction; RIG-I, retinoic acid-inducible gene I; ROS, reactive oxygen species; SAVI, STING-associated vasculopathy with onset in infancy; SLE, systemic lupus erythematosus; STAT, signal transducer and activator of transcription; STING, stimulator of interferon genes; TBI, traumatic brain injury; TBK1, tank-binding kinase 1; TFAM, transcription factor A, mitochondrial; TLR, toll-like receptor; TUNEL, terminal deoxynucleotidyl transferase dUTP nick end labeling; VEGF, vascular endothelial growth factor; WT, wildtype

Declarations

Ethics Approval and Consent to Participate

Not applicable.

Consent for Publication

Not applicable.

Availability of Data and Materials

Raw image files are available at https://data.mendeley.com/datasets/sgc2fv66s4/draft?a=a77409d6-e68f-4e66-af8c-a96c27b9c4e6

Competing Interests

The authors declare that they have no competing interests.

Funding

This work was supported by the National Institute of Neurological Disorders and Stroke of the National Institutes of Health, R01NS096281 and R01NS121103 (M.H.T.), Commonwealth Health Research Board #208-05-20 (A.M.P.), and departmental start-up funds (A.M.P.).

Author Contributions

L.E.F. wrote the first draft, performed experiments. and analyzed data. J.J., E.K.G.B, E.S., S.P, E.J.A.K., J.C., S.P., T.C.T., R.D.S., and X.W. performed experiments and analyzed data. I.C.A. provided the *Nlrx1*$^{-/-}$ mice and analyzed data. M.H.T designed the project and analyzed data. A.M.P. designed the project, performed experiments, analyzed data, and wrote the manuscript. All authors read, edited, and approved the manuscript.

Acknowledgements

We would like to thank Dr. Jenny P.Y. Ting (UNC Chapel Hill) for providing *Nlrx1*$^{-/-}$ mice.

References

1. Roozenbeek B, Maas AIR, Menon DK. Changing patterns in the epidemiology of traumatic brain injury. Nat Rev Neurol [Internet]. 2013 [cited 2019 Mar 24];9:231–6. Available from: http://www.nature.com/articles/nrneurol.2013.22

2. Greve MW, Zink BJ. Pathophysiology of Traumatic Brain Injury. Mt SINAI J Med. 2009;76:97–104.

3. Werner C, Engelhard K. Pathophysiology of traumatic brain injury. Br J Anaesth. 2007;99:4–9.

4. Simon DW, McGeachy MJ, Bayır H, Clark RSB, Loane DJ, Kochanek PM. The far-reaching scope of neuroinflammation after traumatic brain injury. Nat Rev Neurol [Internet]. NIH Public Access; 2017 [cited 2019 Mar 24];13:171–91. Available from: http://www.ncbi.nlm.nih.gov/pubmed/28186177

5. Frugier T, Morganti-Kossmann MC, O'Reilly D, McLean CA. In situ detection of inflammatory mediators in post mortem human brain tissue after traumatic injury. J Neurotrauma. 2010;27:497–507.

6. Karve IP, Zhang M, Habgood M, Frugier T, Brody KM, Sashindranath M, et al. Ablation of type-1 IFN signaling in hematopoietic cells confers protection following traumatic brain injury. eNeuro [Internet]. Society for Neuroscience; 2016 [cited 2021 Jun 7];3:89–93. Available from: https://pubmed.ncbi.nlm.nih.gov/27022620/

7. Lagraoui M, Latoche JR, Cartwright NG, Sukumar G, Dalgard CL, Schaefer BC. Controlled cortical impact and craniotomy induce strikingly similar profiles of inflammatory gene expression, but with distinct kinetics. Front Neurol. 2012;

8. Abe T, Marutani Y, Shoji I. Cytosolic DNA-sensing immune response and viral infection.

505 Microbiol Immunol. 2019;63:51–64.
506 9. Trinchieri G. Type I interferon: friend or foe? J Exp Med [Internet]. The Rockefeller
507 University Press; 2010 [cited 2019 Mar 25];207:2053. Available from:
508 http://www.ncbi.nlm.nih.gov/pubmed/20837696
509 10. Ivashkiv LB, Donlin LT. Regulation of type I interferon responses. Nat Rev Immunol
510 [Internet]. Nature Publishing Group; 2014 [cited 2019 Mar 25];14:36–49. Available from:
511 http://www.nature.com/articles/nri3581
512 11. Zhang C, Shang G, Gui X, Zhang X, Bai X, Chen ZJ. Structural basis of STING binding with
513 and phosphorylation by TBK1. Nature [Internet]. Nature Publishing Group; 2019 [cited 2019 Jul
514 24];567:394–8. Available from: http://www.nature.com/articles/s41586-019-1000-2
515 12. Shang G, Zhang C, Chen ZJ, Bai X chen, Zhang X. Cryo-EM structures of STING reveal its
516 mechanism of activation by cyclic GMP–AMP. Nature. 2019.
517 13. West AP, Khoury-Hanold W, Staron M, Tal MC, Pineda CM, Lang SM, et al. Mitochondrial
518 DNA stress primes the antiviral innate immune response. Nature [Internet]. 2015 [cited 2018
519 Dec 11];520. Available from: http://www.nature.com/articles/nature14156
520 14. Sun L, Wu J, Du F, Chen X, Chen ZJ. Cyclic GMP-AMP synthase is a cytosolic DNA sensor
521 that activates the type I interferon pathway. Science [Internet]. NIH Public Access; 2013 [cited
522 2018 Nov 15];339:786–91. Available from: http://www.ncbi.nlm.nih.gov/pubmed/23258413
523 15. Seth RB, Sun L, Ea C-K, Chen ZJ. Identification and Characterization of MAVS, a
524 Mitochondrial Antiviral Signaling Protein that Activates NF-κB and IRF3. Cell. Cell Press;
525 2005;122:669–82.
526 16. Ishikawa H, Barber GN. STING is an endoplasmic reticulum adaptor that facilitates innate
527 immune signalling. Nature. Nature Publishing Group; 2008;455:674–8.

17. Barber GN. STING-dependent cytosolic DNA sensing pathways. Trends Immunol [Internet]. Elsevier Current Trends; 2014 [cited 2019 Feb 28];35:88–93. Available from: https://www.sciencedirect.com/science/article/pii/S147149061300166X?via%3Dihub

18. Abdullah A, Zhang M, Frugier T, Bedoui S, Taylor JM, Crack PJ. STING-mediated type-I interferons contribute to the neuroinflammatory process and detrimental effects following traumatic brain injury. J Neuroinflammation. BioMed Central Ltd.; 2018;15.

19. Li Q, Cao Y, Dang C, Han B, Han R, Ma H, et al. Inhibition of double-strand DNA-sensing cGAS ameliorates brain injury after ischemic stroke. EMBO Mol Med. 2020;

20. Barrett JP, Henry RJ, Ann Shirey K, Doran SJ, Makarevich OD, Ritzel RR, et al. Interferon-β plays a detrimental role in experimental traumatic brain injury by enhancing neuroinflammation that drives chronic neurodegeneration. J Neurosci. Society for Neuroscience; 2020;2516–9.

21. Sen T, Saha P, Gupta R, Foley LM, Jiang T, Abakumova OS, et al. Aberrant ER Stress Induced Neuronal-IFNβ Elicits White Matter Injury Due to Microglial Activation and T-Cell Infiltration after TBI. J Neurosci [Internet]. NLM (Medline); 2020 [cited 2021 May 31];40:424–46. Available from: https://doi.org/10.1523/JNEUROSCI.0718-19.2019

22. Dunphy G, Flannery SM, Almine JF, Connolly DJ, Paulus C, Jønsson KL, et al. Non-canonical Activation of the DNA Sensing Adaptor STING by ATM and IFI16 Mediates NF-κB Signaling after Nuclear DNA Damage. Mol Cell [Internet]. Elsevier; 2018 [cited 2019 Jul 8];71:745-760.e5. Available from: http://www.ncbi.nlm.nih.gov/pubmed/30193098

23. Unterholzner L, Dunphy G. cGAS-independent STING activation in response to DNA damage. Mol Cell Oncol [Internet]. Taylor & Francis; 2019 [cited 2019 Jul 8];6:1558682. Available from: https://www.tandfonline.com/doi/full/10.1080/23723556.2018.1558682

24. Jassam YN, Izzy S, Whalen M, McGavern DB, El Khoury J. Neuroimmunology of Traumatic Brain Injury: Time for a Paradigm Shift. Neuron. Cell Press; 2017. p. 1246–65.

25. Schneider WM, Chevillotte MD, Rice CM. Interferon-Stimulated Genes: A Complex Web of Host Defenses. Annu Rev Immunol. 2014;

26. Ma F, Li B, Yu Y, Iyer SS, Sun M, Cheng G. Positive feedback regulation of type I interferon by the interferon-stimulated gene STING. EMBO Rep. 2015;

27. McArthur K, Whitehead LW, Heddleston JM, Li L, Padman BS, Oorschot V, et al. BAK/BAX macropores facilitate mitochondrial herniation and mtDNA efflux during apoptosis. Science (80-) [Internet]. American Association for the Advancement of Science; 2018 [cited 2021 Jun 2];359. Available from: https://pubmed.ncbi.nlm.nih.gov/29472455/

28. Kilbaugh TJ, Lvova M, Karlsson M, Zhang Z, Leipzig J, Wallace DC, et al. Peripheral blood mitochondrial DNA as a biomarker of cerebral mitochondrial dysfunction following traumatic brain injury in a porcine model. PLoS One. Public Library of Science; 2015;10.

29. Walko TD, Bola RA, Hong JD, Au AK, Bell MJ, Kochanek PM, et al. Cerebrospinal fluid mitochondrial DNA: A novel DAMP in pediatric traumatic brain injury. Shock. Lippincott Williams and Wilkins; 2014;41:499–503.

30. Urbonaviciute V, Fürnrohr BG, Meister S, Munoz L, Heyder P, De Marchis F, et al. Induction of inflammatory and immune responses by HMGB1-nucleosome complexes: Implications for the pathogenesis of SLE. J Exp Med [Internet]. The Rockefeller University Press; 2008 [cited 2021 May 31];205:3007–18. Available from: www.jem.org/cgi/doi/10.1084/jem.20081165

31. Pisetsky DS. The complex role of DNA, histones and HMGB1 in the pathogenesis of SLE. Autoimmunity [Internet]. Informa Healthcare; 2014 [cited 2021 May 31];47:487–93. Available

574 from: https://pubmed.ncbi.nlm.nih.gov/24916843/
575 32. Andreeva L, Hiller B, Kostrewa D, Lässig C, De Oliveira Mann CC, Jan Drexler D, et al.
576 CGAS senses long and HMGB/TFAM-bound U-turn DNA by forming protein-DNA ladders.
577 Nature [Internet]. Nature Publishing Group; 2017 [cited 2021 May 27];549:394–8. Available
578 from: https://www.nature.com/articles/nature23890
579 33. Bonaldi T, Talamo F, Scaffidi P, Ferrera D, Porto A, Bachi A, et al. Monocytic cells
580 hyperacetylate chromatin protein HMGB1 to redirect it towards secretion. EMBO J [Internet].
581 EMBO J; 2003 [cited 2021 Jun 7];22:5551–60. Available from:
582 https://pubmed.ncbi.nlm.nih.gov/14532127/
583 34. Wu J, Sun L, Chen X, Du F, Shi H, Chen C, et al. Cyclic GMP-AMP is an endogenous
584 second messenger in innate immune signaling by cytosolic DNA. Science (80-) [Internet].
585 American Association for the Advancement of Science; 2013 [cited 2021 May 27];339:826–30.
586 Available from: https://pubmed.ncbi.nlm.nih.gov/23258412/
587 35. Chu T-T, Tu X, Yang K, Wu J, Repa JJ, Yan N. Tonic prime-boost of STING signalling
588 mediates Niemann–Pick disease type C. Nat 2021 [Internet]. Nature Publishing Group; 2021
589 [cited 2021 Aug 17];1–6. Available from: https://www.nature.com/articles/s41586-021-03762-2
590 36. Luksch H, Stinson WA, Platt DJ, Qian W, Kalugotla G, Miner CA, et al. STING-associated
591 lung disease in mice relies on T cells but not type I interferon. J Allergy Clin Immunol. Mosby;
592 2019;144:254-266.e8.
593 37. Grasl-Kraupp B, Ruttkay-Nedecky B, Koudelka H, Bukowska K, Bursch W, Schulte-
594 Hermann R. In situ detection of fragmented DNA (tunel assay) fails to discriminate among
595 apoptosis, necrosis, and autolytic cell death: A cautionary note. Hepatology. 1995;
596 38. Shlosberg D, Benifla M, Kaufer D, Friedman A. Blood-brain barrier breakdown as a

therapeutic target in traumatic brain injury [Internet]. Nat. Rev. Neurol. Nature Publishing Group; 2010 [cited 2021 Jun 1]. p. 393–403. Available from: https://www.nature.com/articles/nrneurol.2010.74

39. Alluri H, Wiggins-Dohlvik K, Davis ML, Huang JH, Tharakan B. Blood–brain barrier dysfunction following traumatic brain injury [Internet]. Metab. Brain Dis. Springer New York LLC; 2015 [cited 2021 Jun 1]. p. 1093–104. Available from: https://link.springer.com/article/10.1007/s11011-015-9651-7

40. Cash A, Theus MH. Mechanisms of blood–brain barrier dysfunction in traumatic brain injury [Internet]. Int. J. Mol. Sci. MDPI AG; 2020 [cited 2021 Jun 1]. p. 3344. Available from: https://pubmed.ncbi.nlm.nih.gov/32397302/

41. Zhang D, Liu C, Li H, Jiao J. Deficiency of STING Signaling in Embryonic Cerebral Cortex Leads to Neurogenic Abnormalities and Autistic-Like Behaviors. Adv Sci [Internet]. John Wiley & Sons, Ltd; 2020 [cited 2021 Aug 25];7:2002117. Available from: https://onlinelibrary.wiley.com/doi/full/10.1002/advs.202002117

42. Nazmi A, Mukhopadhyay R, Dutta K, Basu A. STING Mediates Neuronal Innate Immune Response Following Japanese Encephalitis Virus Infection. Sci Reports 2012 21 [Internet]. Nature Publishing Group; 2012 [cited 2021 Aug 25];2:1–10. Available from: https://www.nature.com/articles/srep00347

43. Holt LM, Olsen ML. Novel applications of magnetic cell sorting to analyze cell-type specific gene and protein expression in the central nervous system. PLoS One. 2016;

44. Holt LM, Stoyanof ST, Olsen ML. Magnetic Cell Sorting for In Vivo and In Vitro Astrocyte, Neuron, and Microglia Analysis. Curr Protoc Neurosci [Internet]. Blackwell Publishing Inc.; 2019 [cited 2020 Mar 9];88. Available from:

https://onlinelibrary.wiley.com/doi/abs/10.1002/cpns.71

45. Theus MH, Brickler T, Meza A, Coutermarsh-Ott S, Hazy A, Gris D, et al. Loss of NLRX1 Exacerbates Neural Tissue Damage and NF-kB Signaling following Brain Injury. J Immunol. 2017;

46. Guo H, König R, Deng M, Riess M, Mo J, Zhang L, et al. NLRX1 Sequesters STING to Negatively Regulate the Interferon Response, Thereby Facilitating the Replication of HIV-1 and DNA Viruses. Cell Host Microbe. 2016;

47. Goto A, Okado K, Martins N, Cai H, Barbier V, Lamiable O, et al. The Kinase IKKβ Regulates a STING- and NF-κB-Dependent Antiviral Response Pathway in Drosophila. Immunity. 2018;

48. Martin M, Hiroyasu A, Guzman RM, Roberts SA, Goodman AG. Analysis of Drosophila STING Reveals an Evolutionarily Conserved Antimicrobial Function. Cell Rep. 2018;

49. Liu Y, Gordesky-Gold B, Leney-Greene M, Weinbren NL, Tudor M, Cherry S. Inflammation-Induced, STING-Dependent Autophagy Restricts Zika Virus Infection in the Drosophila Brain. Cell Host Microbe. 2018;

50. Reinert LS, Lopušná K, Winther H, Sun C, Thomsen MK, Nandakumar R, et al. Sensing of HSV-1 by the cGAS-STING pathway in microglia orchestrates antiviral defence in the CNS. Nat Commun. Nature Publishing Group; 2016;7:1–12.

51. Reinert LS, Rashidi AS, Tran DN, Katzilieris-Petras G, Hvidt AK, Gohr M, et al. Brain immune cells undergo cGAS/STING-dependent apoptosis during herpes simplex virus type 1 infection to limit type I IFN production. J Clin Invest. American Society for Clinical Investigation; 2021;131.

52. Mathur V, Burai R, Vest RT, Bonanno LN, Lehallier B, Zardeneta ME, et al. Activation of

643 the STING-Dependent Type I Interferon Response Reduces Microglial Reactivity and
644 Neuroinflammation. Neuron. 2017;
645 53. Almine JF, O'Hare CAJ, Dunphy G, Haga IR, Naik RJ, Atrih A, et al. IFI16 and cGAS
646 cooperate in the activation of STING during DNA sensing in human keratinocytes. Nat Commun
647 [Internet]. Nature Publishing Group; 2017 [cited 2021 Jun 3];8:1–15. Available from:
648 www.nature.com/naturecommunications
649 54. Storek KM, Gertsvolf NA, Ohlson MB, Monack DM. cGAS and Ifi204 Cooperate To
650 Produce Type I IFNs in Response to Francisella Infection . J Immunol [Internet]. The American
651 Association of Immunologists; 2015 [cited 2021 Jun 3];194:3236–45. Available from:
652 https://pubmed.ncbi.nlm.nih.gov/25710914/
653 55. Ahn J, Son S, Oliveira SC, Barber GN. STING-Dependent Signaling Underlies IL-10
654 Controlled Inflammatory Colitis. Cell Rep [Internet]. 2017 [cited 2019 Feb 28];21:3873–84.
655 Available from: http://www.ncbi.nlm.nih.gov/pubmed/29281834
656 56. Motwani M, McGowan J, Antonovitch J, Gao KMJ, Jiang Z, Sharma S, et al. cGAS-STING
657 Pathway Does Not Promote Autoimmunity in Murine Models of SLE. Front Immunol [Internet].
658 Frontiers Media S.A.; 2021 [cited 2021 Jun 3];12. Available from:
659 https://pubmed.ncbi.nlm.nih.gov/33854495/
660 57. Thim-uam A, Prabakaran T, Tansakul M, Makjaroen J, Wongkongkathep P, Chantaravisoot
661 N, et al. STING Mediates Lupus via the Activation of Conventional Dendritic Cell Maturation
662 and Plasmacytoid Dendritic Cell Differentiation. iScience. Elsevier Inc.; 2020;23:101530.
663 58. Sharma S, Campbell AM, Chan J, Schattgen SA, Orlowski GM, Nayar R, et al. Suppression
664 of systemic autoimmunity by the innate immune adaptor STING. Proc Natl Acad Sci U S A
665 [Internet]. National Academy of Sciences; 2015 [cited 2021 Jun 3];112:E710–7. Available from:

https://pubmed.ncbi.nlm.nih.gov/25646421/

59. Liu Y, Jesus AA, Marrero B, Yang D, Ramsey SE, Montealegre Sanchez GA, et al. Activated STING in a Vascular and Pulmonary Syndrome. N Engl J Med [Internet]. New England Journal of Medicine (NEJM/MMS); 2014 [cited 2021 Jun 3];371:507–18. Available from: https://pubmed.ncbi.nlm.nih.gov/25029335/

60. McKee CA, Lukens JR. Emerging roles for the immune system in traumatic brain injury [Internet]. Front. Immunol. Frontiers Media S.A.; 2016 [cited 2021 Jun 3]. Available from: https://pubmed.ncbi.nlm.nih.gov/27994591/

61. Abe T, Barber GN. Cytosolic-DNA-Mediated, STING-Dependent Proinflammatory Gene Induction Necessitates Canonical NF- B Activation through TBK1. J Virol [Internet]. 2014 [cited 2019 Feb 28];88:5328–41. Available from: http://www.ncbi.nlm.nih.gov/pubmed/24600004

62. Stetson DB, Medzhitov R. Recognition of cytosolic DNA activates an IRF3-dependent innate immune response. Immunity. 2006;

63. Tanaka Y, Chen ZJ. STING specifies IRF3 phosphorylation by TBK1 in the cytosolic DNA signaling pathway. Sci Signal. 2012;

64. Zhong B, Yang Y, Li S, Wang YY, Li Y, Diao F, et al. The Adaptor Protein MITA Links Virus-Sensing Receptors to IRF3 Transcription Factor Activation. Immunity. 2008;

65. Yum S, Li M, Fang Y, Chen ZJ. TBK1 recruitment to STING activates both IRF3 and NF-κB that mediate immune defense against tumors and viral infections. Proc Natl Acad Sci U S A [Internet]. National Academy of Sciences; 2021 [cited 2021 Jun 1];118. Available from: https://www.pnas.org/content/118/14/e2100225118

66. Yu CH, Davidson S, Harapas CR, Hilton JB, Mlodzianoski MJ, Laohamonthonkul P, et al. TDP-43 Triggers Mitochondrial DNA Release via mPTP to Activate cGAS/STING in ALS. Cell

689 [Internet]. Cell Press; 2020 [cited 2021 Jun 4];183:636-649.e18. Available from:
690 https://pubmed.ncbi.nlm.nih.gov/33031745/
691 67. Riley JS, Quarato G, Cloix C, Lopez J, O'Prey J, Pearson M, et al. Mitochondrial inner
692 membrane permeabilisation enables mt DNA release during apoptosis . EMBO J [Internet].
693 EMBO; 2018 [cited 2021 Jun 4];37. Available from: https://pubmed.ncbi.nlm.nih.gov/30049712/
694 68. Helle SCJ, Feng Q, Aebersold MJ, Hirt L, Grüter RR, Vahid A, et al. Mechanical force
695 induces mitochondrial fission. Elife. eLife Sciences Publications Ltd; 2017;6.
696 69. Fischer TD, Hylin MJ, Zhao J, Moore AN, Waxham MN, Dash PK. Altered mitochondrial
697 dynamics and TBI pathophysiology. Front Syst Neurosci [Internet]. Frontiers Media S.A.; 2016
698 [cited 2021 Jun 4];10:29. Available from: www.frontiersin.org
699 70. Han J, Fan Y, Zhou K, Blomgren K, Harris RA. Uncovering sex differences of rodent
700 microglia. J Neuroinflammation 2021 181 [Internet]. BioMed Central; 2021 [cited 2021 Aug
701 25];18:1–11. Available from:
702 https://jneuroinflammation.biomedcentral.com/articles/10.1186/s12974-021-02124-z
703 71. Villa A, Gelosa P, Castiglioni L, Cimino M, Rizzi N, Pepe G, et al. Sex-Specific Features of
704 Microglia from Adult Mice. Cell Rep [Internet]. Elsevier; 2018 [cited 2021 Aug 25];23:3501.
705 Available from: /pmc/articles/PMC6024879/
706 72. Klein SL, Flanagan KL. Sex differences in immune responses. Nat Rev Immunol 2016 1610
707 [Internet]. Nature Publishing Group; 2016 [cited 2021 Aug 25];16:626–38. Available from:
708 https://www.nature.com/articles/nri.2016.90
709 73. Sauer JD, Sotelo-Troha K, Von Moltke J, Monroe KM, Rae CS, Brubaker SW, et al. The N-
710 ethyl-N-nitrosourea-induced Goldenticket mouse mutant reveals an essential function of sting in
711 the in vivo interferon response to Listeria monocytogenes and cyclic dinucleotides. Infect

Immun. Infect Immun; 2011;79:688–94.

74. Allen IC, Moore CB, Schneider M, Lei Y, Davis BK, Scull MA, et al. NLRX1 Protein Attenuates Inflammatory Responses to Infection by Interfering with the RIG-I-MAVS and TRAF6-NF-κB Signaling Pathways. Immunity. Cell Press; 2011;34:854–65.

75. Brickler T, Gresham K, Meza A, Coutermarsh-Ott S, Williams TM, Rothschild DE, et al. Nonessential role for the NLRP1 inflammasome complex in a murine model of traumatic brain injury. Mediators Inflamm. 2016;

76. Theus MH, Ricard J, Bethea JR, Liebl DJ. EphB3 limits the expansion of neural progenitor cells in the subventricular zone by regulating p53 during homeostasis and following traumatic brain injury. Stem Cells. 2010;

77. Schmittgen TD, Livak KJ. Analyzing real-time PCR data by the comparative CT method. Nat Protoc. 2008;3:1101–8.

78. Holt LM, Stoyanof ST, Olsen ML. Magnetic cell sorting for in vivo and in vitro astrocyte, neuron, and microglia analysis. Curr Protoc Neurosci [Internet]. NIH Public Access; 2019 [cited 2021 Aug 18];88:e71. Available from: /pmc/articles/PMC6653683/

Figure Legends

Figure 1: The immune response to TBI is biphasic.

Cytokine and interferon-stimulated gene (ISG) expression profiled at 2 hours (**a**), 4 hours (**b**), and 24 hours (**c**) after injury or sham surgery in male CD-1 mice. (**d**) mRNA expression of STING in the ipsilateral cortex 2, 4, and 24 hours after injury or sham surgery. Gene expression was normalized to GAPDH. n = 5-7 per group. Data presented as mean ± SEM. *p < 0.05, **p < 0.01, ***p < 0.001, ****p < 0.0001.

Figure 2: mtDNA is present in the cytosol as a possible trigger for cGAS-STING activation after TBI.

(a-e) The cytosol from cells in the ipsilateral and contralateral hemisphere of WT animals was isolated at the specified time points. **(a)** Diagram of mtDNA showing primer sets for ND1 and COX1. **(b)** Western blot of whole cell lysate (WCL), cell pellet, and isolated cytosol to confirm cytosolic purity. Mitofusin 2 (MFN2) was used to identity mitochondria, alpha-tubulin was used for detecting cytosol, and histone H3 indicated the nuclear fraction. **(c)** mtDNA was directly detected in the cytosol via qPCR at 2, 4, and 24 hours post-TBI. **(d)** Representative western blotting of the DNA-binding protein high mobility group box protein 1 (HMGB1) in the cytosol 2 hours post-TBI. **(e)** Quantification of HMGB1 western blot normalized to alpha-tubulin. n = 5 per group for all experiments. Data presented as mean ± SEM. *$p < 0.05$.

Figure 3: Loss of endogenous cGAS and STING decreases lesion volume and cell death after TBI.

(**a**) Quantification of lesion volume in Cresyl violet stained WT, *STING*$^{-/-}$, and *cGAS*$^{-/-}$ brains 24hrs after CCI injury. n = 6-11 per genotype. (**b-d**) Representative images of Cresyl violet stained brains at 4x magnification. Dashed line indicates lesion site. Scale bar = 1mm. (**e**) Quantification of density of apoptotic cells (indicated by cells labeled with TUNEL per mm^3) in the lesion site 24 hours after injury in WT, *STING*$^{-/-}$, and *cGAS*$^{-/-}$ mice. (**f**) Density of apoptotic neurons (indicated by cells positive for both TUNEL and Nissl per mm^3) in the lesion site 24hrs after injury in WT, STING$^{-/-}$, and *cGAS*$^{-/-}$ mice. n = 6-12 per group. (**g**) Quantification of Evans blue absorbance (O.D. 610nm) from contralateral and ipsilateral cortex 24hrs after injury in WT, *cGAS*$^{-/-}$, and *STING*$^{-/-}$ mice. n = 6-7 per genotype. **(h)** Representative confocal images of TUNEL (green), Nissl (red),

and DAPI (blue) at 20x magnification of ipsilateral hemisphere of CCI-injured WT, STING$^{-/-}$, and cGAS$^{-/-}$ animals. Scale bar = 1mm Data presented as mean ± SEM. *p < 0.05, **p < 0.01, ***p < 0.001, ****p < 0.0001.

Figure 4: Loss of cGAS-STING blunts the innate immune response to TBI.

Quantified mRNA expression of (**a**) *Il10,* (**b**) *Il6*, (**c**) *MCP1*, (**d**) *IFNA4*, and (**e**) *IFNB1* assessed by qPCR at 24hrs post-injury in wildtype, *STING$^{-/-}$,* and *cGAS$^{-/-}$* cortices. Gene expression normalized to GAPDH. n = 5-6 per group. Data presented as mean ± SEM. *p <0.05, **p<0.01, ****p<0.0001.

Figure 5: Microglia are the predominant cell type expressing cGAS and STING in the CNS.

Cell type specific populations were isolated from naïve (uninjured) WT male animals. (**a**) mRNA expression of gap junction associated protein 1 (*Gja1*), transmembrane protein 119 (*TMEM119*), and vascular-endothelial cadherin (*VE-cadherin*), genes characteristic of astrocytes, microglia, and endothelial cells, respectively. Data is normalized to the characteristic (control) cell type to show purity of isolated populations. # = p < 0.0001 compared to control cell type. **(b)** *cGAS* and (**c**) *STING* mRNA expression in isolated cell types and whole cortex. n = 3-5 per cell type. ****p<0.0001.

Figure 6: NLRX1 negatively restricts cGAS-STING activation after injury.

(**a**) Representative western blotting of phosphorylated STING, STING, and alpha tubulin in WT and NLRX1 KO cortical tissue 3 days post-injury or sham surgery. (**b**) Quantification of pSTING/STING, normalized to alpha tubulin shown in (**a**). mRNA expression of (**c**) *Il10*, (**d**) *Il6*,

(**e**) *MCP1*, (**f**) *IFNA4*, and (**g**) *IFNB1* assessed by qPCR at 24hrs post-injury in wildtype and *NLRX1*$^{-/-}$ cortices. Gene expression normalized to GAPDH. n = 5-7 per group. Data presented as mean ± SEM. *p < 0.05, **p < 0.01, ***p < 0.001.

Supplemental Figure 1: Western blotting to confirm cGAS and STING KO.

(**a-b**) Representative western blot for STING and cGAS protein in brain homogenates from WT, *STING*$^{-/-}$, and *cGAS*$^{-/-}$ mice. Each lane represents an individual animal.

Supplemental Figure 2: cGAS$^{-/-}$ mice show reduced motor deficit after TBI.

Rotarod performance compared to baseline for cGAS$^{-/-}$ and WT animals 4-14 days following sham (**a**) or CCI (**b**) surgery. n = 5 per genotype for (**a**) and n = 15 per genotype for (**b**). (**c**) Lesion volume of WT, *STING*$^{-/-}$, and *cGAS*$^{-/-}$ brains 14dpi. (**d**) Representative Cresyl violet stained WT, STING$^{-/-}$, and cGAS$^{-/-}$ brains 14dpi. Dashed lines indicate lesion site. Scale bar = 1mm. (**e**) mRNA expression of *IFNA4, IFNB1* and *Il6* assessed via qPCR 14dpi or sham surgery for WT and cGAS KO animals. n = 5-7 per group. Data presented as mean ± SEM. Two-way ANOVA used for (**a**) and (**b**), one-way ANOVA for (**c**) and (**e**). *p < 0.05, **p < 0.01, ***p < 0.001, ****p<0.0001.

Supplemental Figure 3: Comparison of cytokine expression between ipsilateral sham and contralateral injured tissue. mRNA expression of (**a**) *Il6* and (**b**) *Il10* 2-hours after surgery from the cortices of sham and CCI-injured WT animals. Gene expression was normalized to GAPDH. n = 5-6 per group. Data presented as mean ± SEM.

Supplemental Figure 4: Loss of STING attenuates cytokine and ISG response after injury.

(a-c) Cytokine and interferon-stimulated gene (ISG) expression profiled 24hrs after CCI from the contralateral and ipsilateral hemispheres of STING$^{-/-}$ and WT mice. Cortical expression of (**a**) *CXCL10,* (**b**) *IRF7,* (**c**) *IFIT1,* (**d**) *IFIT3,* (**e**) *STAT1,* (**f**) *STAT2,* (**g**) *RIG-I,* and (**h**) *IFIH1* in WT and STING KO animals 24hrs post-TBI. Gene expression was normalized to GAPDH. n = 5-6 per group. Data presented as mean ± SEM. *p < 0.05, **p < 0.01, ***p < 0.001, ****p < 0.0001.

Figure 1

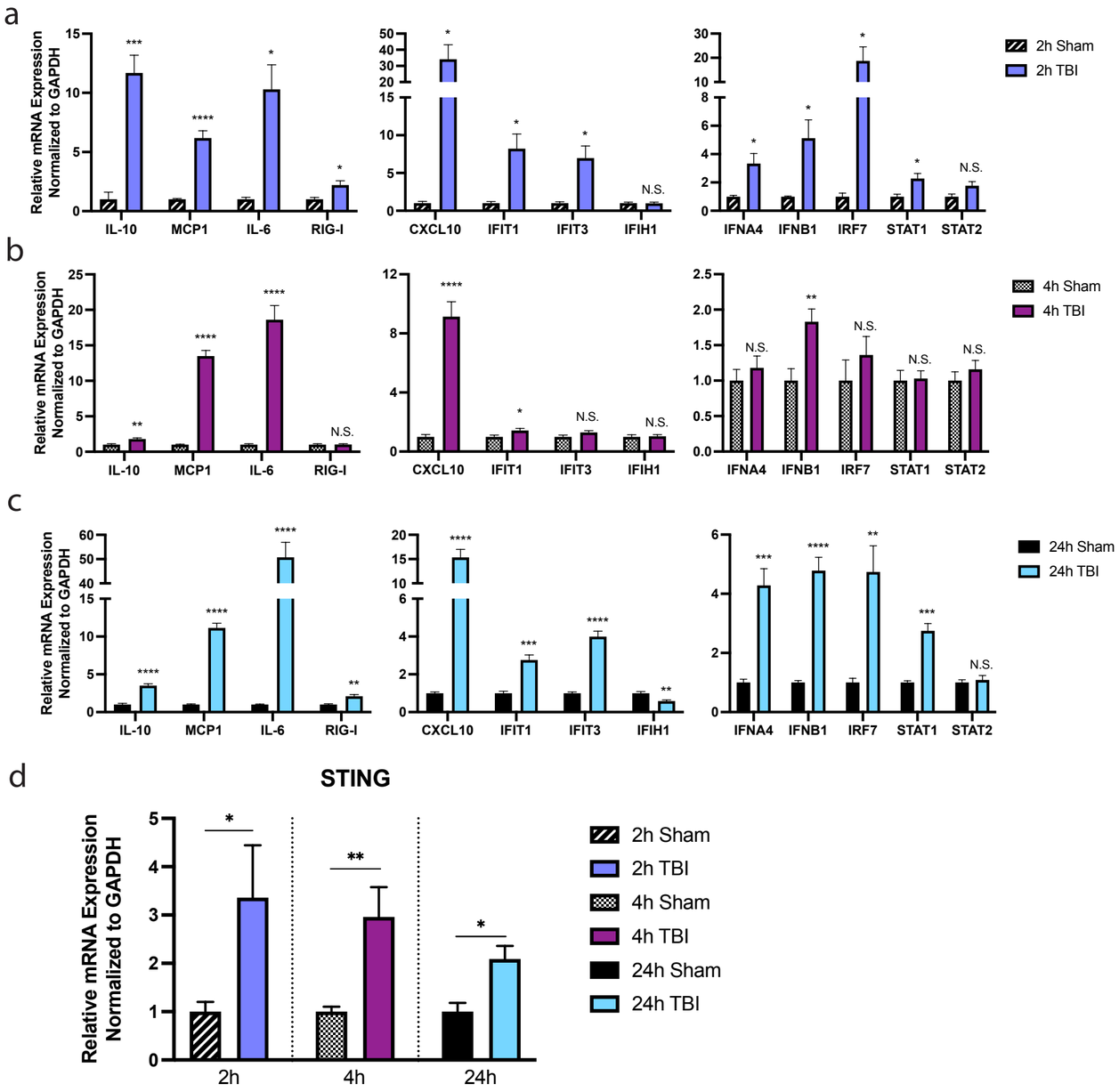
a
Relative mRNA Expression Normalized to GAPDH
IL-10
MCP1
IL-6
RIG-I
CXCL10
IFIT1
IFIT3
IFIH1
IFNA4
IFNB1
IRF7
STAT1
STAT2
N.S.
2h Sham
2h TBI
b
4h Sham
4h TBI
c
24h Sham
24h TBI
d
STING
2h
4h
24h

Figure 2

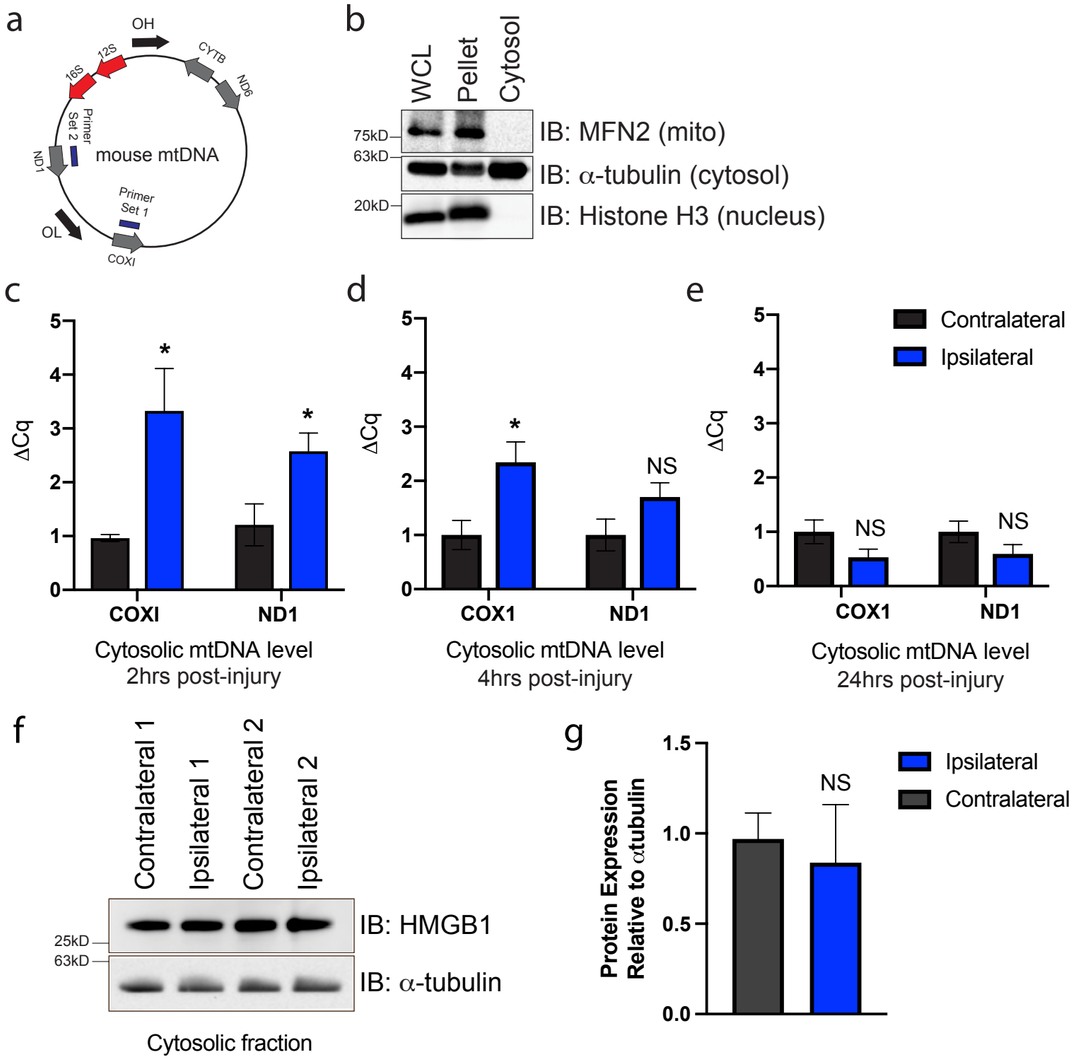
a
OH
12S
16S
CYTB
ND6
Primer Set 2
ND1
mouse mtDNA
Primer Set 1
OL
COXI
b
WCL
Pellet
Cytosol
75kD
63kD
20kD
IB: MFN2 (mito)
IB: α-tubulin (cytosol)
IB: Histone H3 (nucleus)
c
ΔCq
COXI
ND1
Cytosolic mtDNA level
2hrs post-injury
d
ΔCq
NS
COX1
ND1
Cytosolic mtDNA level
4hrs post-injury
e
Contralateral
Ipsilateral
ΔCq
NS
NS
COX1
ND1
Cytosolic mtDNA level
24hrs post-injury
f
Contralateral 1
Ipsilateral 1
Contralateral 2
Ipsilateral 2
25kD
63kD
IB: HMGB1
IB: α-tubulin
Cytosolic fraction
g
Protein Expression Relative to αtubulin
NS
Ipsilateral
Contralateral

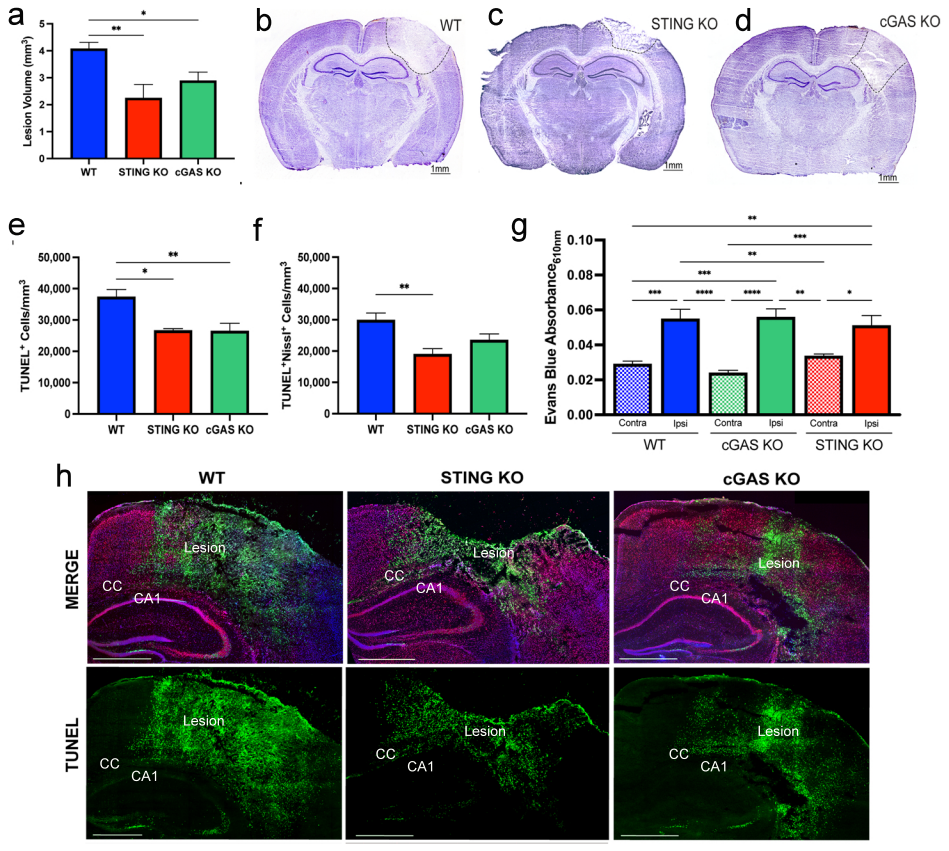
a
Lesion Volume (mm³)
WT
STING KO
cGAS KO
b
WT
c
STING KO
d
cGAS KO
1mm
e
TUNEL⁺ Cells/mm³
f
TUNEL⁺Nissl⁺ Cells/mm³
g
Evans Blue Absorbance₆₁₀nm
Contra
Ipsi
h
MERGE
TUNEL
Lesion
CC
CA1

Figure 4

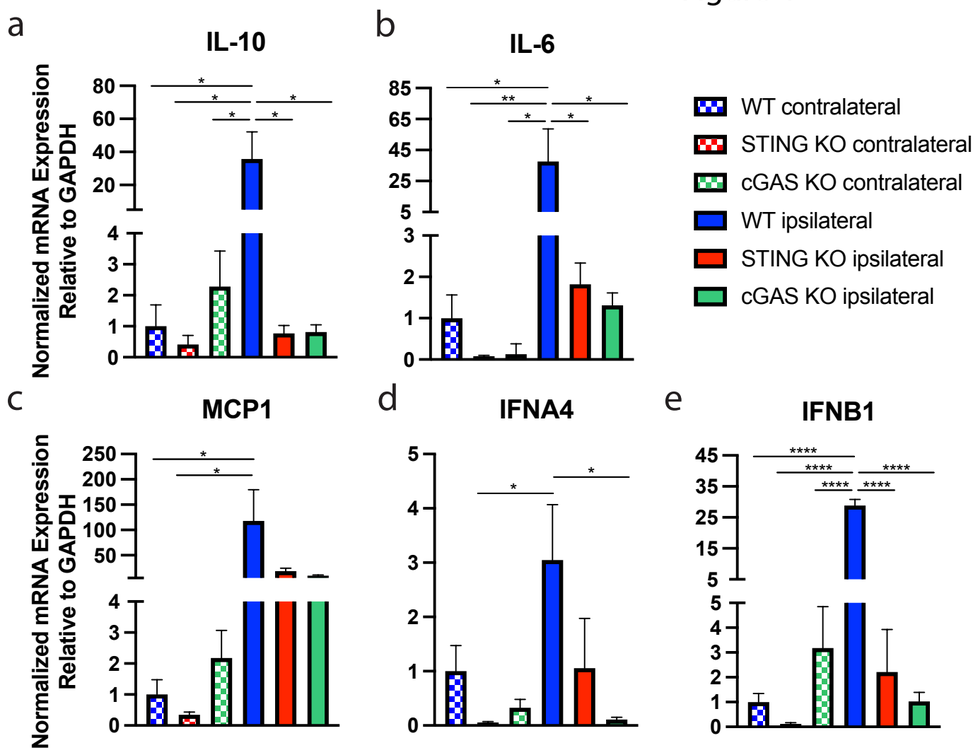
a
IL-10
b
IL-6
Normalized mRNA Expression
Relative to GAPDH
WT contralateral
STING KO contralateral
cGAS KO contralateral
WT ipsilateral
STING KO ipsilateral
cGAS KO ipsilateral
c
MCP1
d
IFNA4
e
IFNB1

Figure 5

a

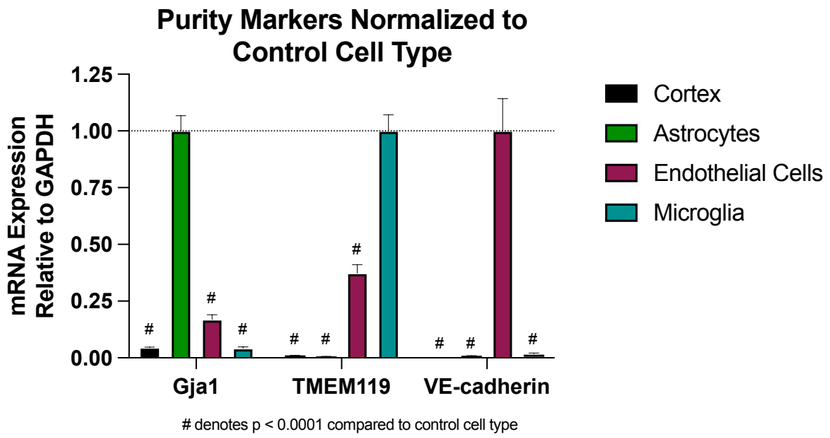
Purity Markers Normalized to Control Cell Type
mRNA Expression Relative to GAPDH
1.25
1.00
0.75
0.50
0.25
0.00
Gja1
TMEM119
VE-cadherin
Cortex
Astrocytes
Endothelial Cells
Microglia
# denotes p < 0.0001 compared to control cell type

b

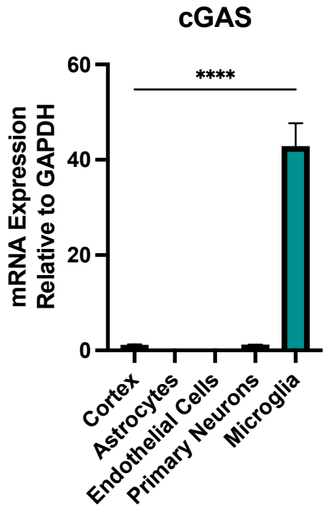
cGAS
mRNA Expression Relative to GAPDH
60
40
20
0
****
Cortex
Astrocytes
Endothelial Cells
Primary Neurons
Microglia

c

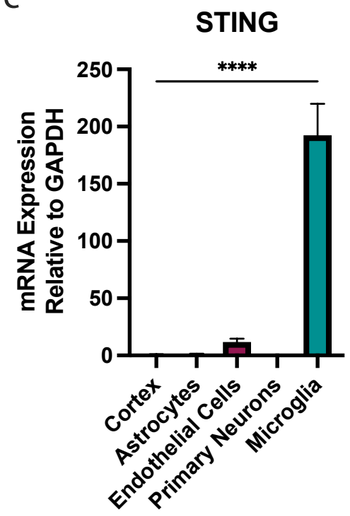
STING
mRNA Expression Relative to GAPDH
250
200
150
100
50
0
****
Cortex
Astrocytes
Endothelial Cells
Primary Neurons
Microglia

Figure 6

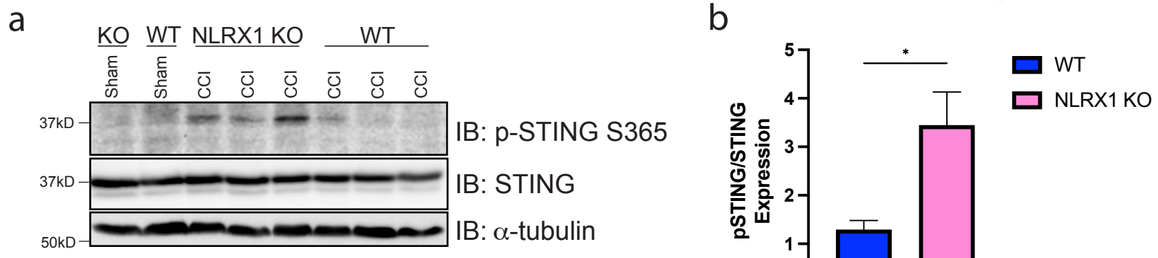
a
KO
WT
NLRX1 KO
WT
Sham
Sham
CCI
CCI
CCI
CCI
CCI
CCI
37kD
37kD
50kD
IB: p-STING S365
IB: STING
IB: α-tubulin

b
pSTING/STING Expression
WT
NLRX1 KO
*

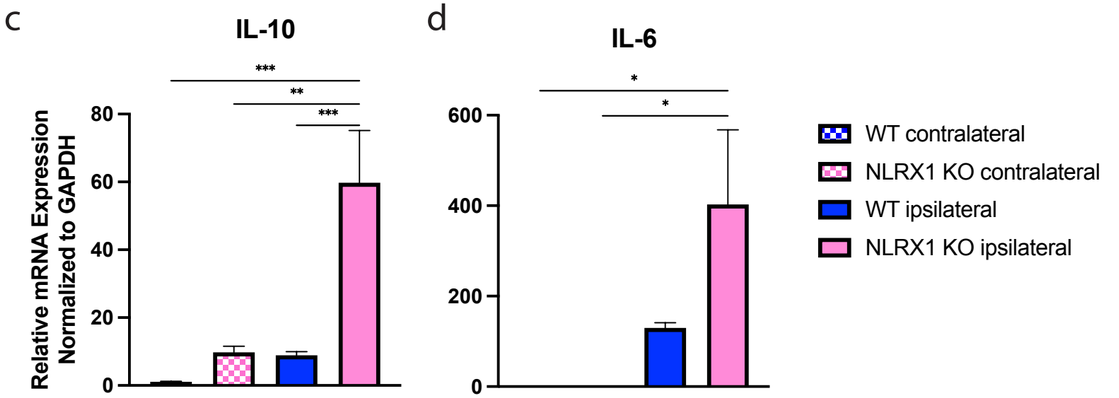
c
IL-10
Relative mRNA Expression Normalized to GAPDH
***
**
***

d
IL-6
*
*

WT contralateral
NLRX1 KO contralateral
WT ipsilateral
NLRX1 KO ipsilateral

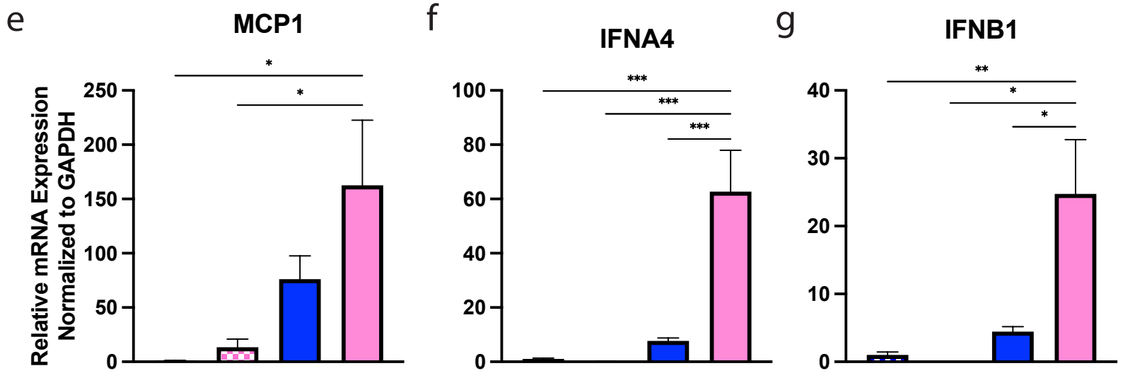
e
MCP1
Relative mRNA Expression Normalized to GAPDH
*
*

f
IFNA4
***
***
***

g
IFNB1
**
*
*

Supplemental Figure 1

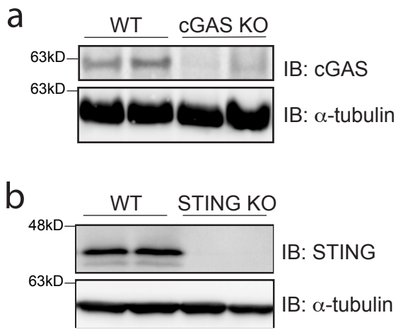

Supplemental Figure 2

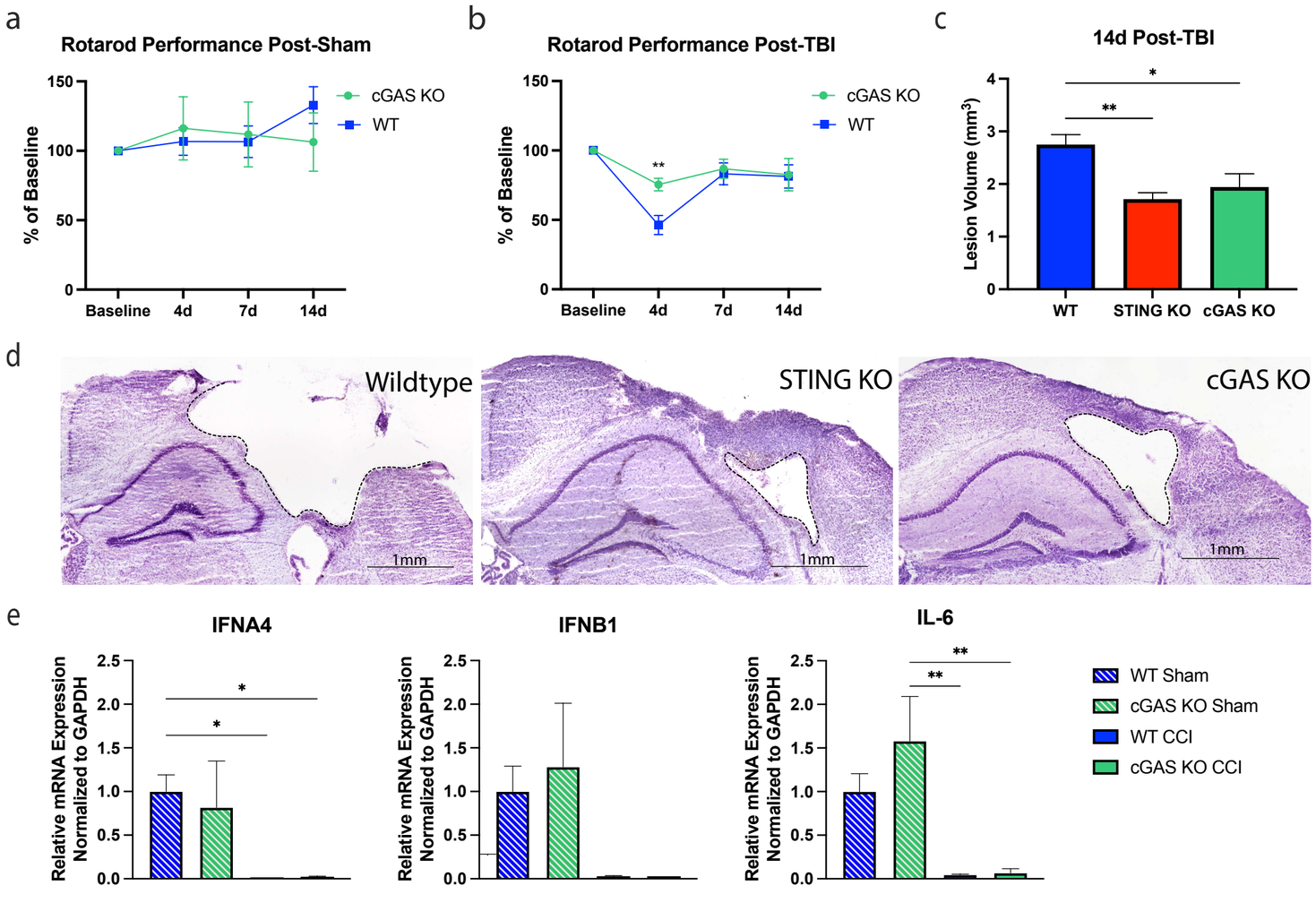

Supplemental Figure 3

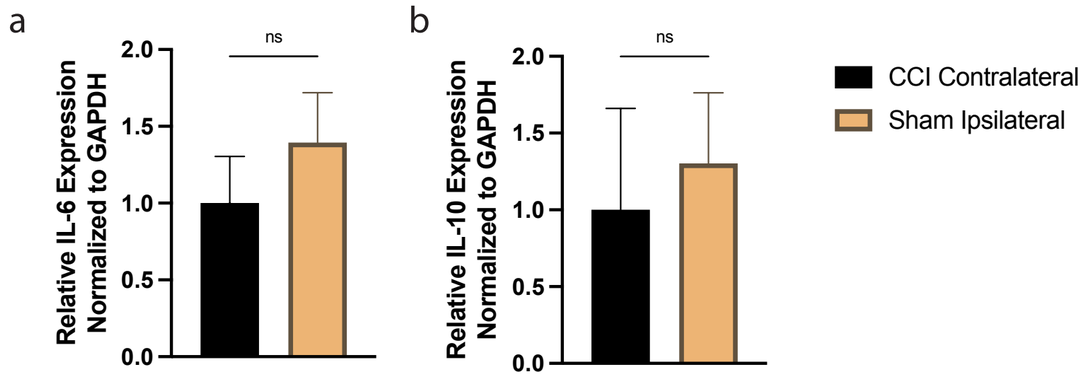

Supplemental Figure 4